ELSEVIER

Coastal Engineering 34 (1998) 243–257

COASTAL ENGINEERING

Hyperbolic mild-slope equations extended to account for rapidly varying topography

Changhoon Lee [a,*], Woo Sun Park [a], Yong-Sik Cho [b], Kyung Doug Suh [c]

[a] *Coastal and Harbor Engineering Research Center, Korea Ocean Research and Development Institute, Ansan P.O. Box 29, Seoul 425-600, South Korea*

[b] *Department of Civil Engineering and Institute of Waterway Industry, Sejong University, 98 Kunja-Dong, Kwangjin-Ku, Seoul 143-747, South Korea*

[c] *Department of Civil Engineering, Seoul National University, Seoul 151-742, South Korea*

Received 26 August 1997; accepted 8 May 1998

Abstract

In this paper, following the procedure outlined by Copeland [Copeland, G.J.M., 1985. A practical alternative to the mild-slope wave equation. Coastal Eng. 9, 125–149.] the elliptic extended refraction–diffraction equation of Massel [Massel, S.R., 1993. Extended refraction–diffraction equation for surface waves. Coastal Eng. 19, 97–126.] is recasted into the form of a pair of first-order equations, which constitute a hyperbolic system. The resultant model, which includes higher-order bottom effect terms proportional to the square of bottom slope and to the bottom curvature, is merely an extension of the Copeland's model to account for a rapidly varying topography. The importance of the higher-order bottom effect terms is examined in terms of relative water depth. The model developed is verified against other numerical or experimental results related to wave reflection from a plane slope with different inclination, from a patch of periodic ripples, and from an arc-shaped bar with different front angle. The relative importance of the higher-order bottom effect terms is also examined for these problems. © 1998 Elsevier Science B.V. All rights reserved.

Keywords: Hyperbolic mild-slope equations; Rapidly varying topography; Numerical model; Bragg reflection

* Corresponding author. Fax: +82-345-408-5823; E-mail: clee@kordi.re.kr

PII S0378-3839(98)00028-3

1. Introduction

The prediction of water wave transformation over an irregular topography is important to coastal engineers who plan, design, construct, and maintain various coastal facilities. In a linear dispersive system, the combined effect of water wave transformations such as refraction, diffraction, shoaling, and reflection can be predicted by the mild-slope equation which was first developed by Berkhoff (1972) without restriction on the water depth. In the derivation of this equation, he assumed a mild slope of the bottom, i.e., $|\nabla h|/kh \ll 1$ (where $\nabla =$ horizontal gradient operator, $k =$ wavenumber, and $h =$ water depth), and thus neglected the terms of second-order bottom effect proportional to $(\nabla h)^2$ and $\nabla^2 h$. Booij (1983) compared the mild-slope equation with a finite element model in terms of the reflection coefficient for the case of monochromatic waves propagating over a plane slope, concluding that the mild-slope equation is sufficiently accurate up to the bottom slope of 1:3.

Recently, the inclusion of the second-order bottom effect terms in the mild-slope equation has been found to yield a more accurate solution, in particular, for a rapidly varying topography such as a steep slope or an undulatory bottom. Massel (1993) and Chamberlain and Porter (1995) used the Galerkin-eigenfunction method to develop an elliptic equation for monochromatic waves. Suh et al. (1997) used the Green's second identity and Lagrangian formula to develop two ultimately equivalent hyperbolic equations for random waves. Without the second-order bottom effect terms, Suh et al.'s equations reduce to the hyperbolic mild-slope equations developed by Smith and Sprinks (1975) and Radder and Dingemans (1985), respectively. For a monochromatic wave, the equation of Suh et al. reduces to that of Massel or Chamberlain and Porter, which in turn, without the second-order bottom effect terms, reduces to the mild-slope equation of Berkhoff.

Compared to an elliptic model, a hyperbolic model offers the advantage of reduced computing time, particularly in a two-dimensional domain, and is able to incorporate the boundaries of arbitrary reflecting intensity as well as refraction and diffraction mechanisms. Nishimura et al. (1983) derived hyperbolic mild-slope equations by vertically integrating the continuity equation and the equation of motion for linear waves. On the other hand, starting from the time-dependent mild-slope equation of Booij (1981), Copeland (1985) derived similar hyperbolic equations using the characteristics of linear waves and the defined volume flux. The equations of Nishimura et al. and Copeland are mathematically equivalent to each other and also to the elliptic mild-slope equation of Berkhoff.

When the bottom topography is simple, the transformation of water waves can be predicted with high accuracy even for the case of abrupt depth change. The first way, which was presented by Booij (1983), is to use the finite element method in solving the Laplace equation with proper boundary conditions. The second way is to assume the bottom topography as a succession of horizontal shelves separated by vertical steps and then match the boundary conditions for continuity of both pressure and horizontal flux at each step discontinuity. The resulting matrix equation can be solved by using the eigenfunction expansion method (Takano, 1960), the variational principle (Miles, 1967), the boundary integral equation method (Yeung, 1975), or the conservation of wave action (Smith, 1983). In this study, the finite element method or the eigenfunction expansion method is employed where appropriate in order to examine the accuracy of the model we develop and the existing Copeland's model.

In the following, we first recast the elliptic formulation of Massel (1993) and Chamberlain and Porter (1995) into a hyperbolic one following the technique of Copeland (1985). Second, we investigate the terms of second-order bottom effect which are included in the present model. Third, in order to verify the better accuracy of the present model compared to the Copeland's model in cases of rapidly varying topography, the two models are applied to the problems of wave reflection from a plane slope with different inclination (Booij, 1983), from a ripple patch (Davies and Heathershaw, 1984), and from an arc-shaped bar with different front angle. The relative importance of the second-order bottom effect terms is also examined for these problems. Finally, major conclusions follow.

2. Development of model equations

The extended refraction–diffraction equation of Massel (1993) with the evanescent modes neglected is given by

$$\nabla \cdot \left(CC_g \nabla \tilde{\phi} \right) + \omega^2 \left\{ \frac{C_g}{C} - R_1 (\nabla h)^2 - R_2 \nabla^2 h \right\} \tilde{\phi} = 0 \tag{1}$$

where $\tilde{\phi}$ is the velocity potential at mean water level, C and C_g are the phase speed and group velocity, respectively, of a wave with the angular frequency, ω, and wavenumber, k, and the parameters R_1 and R_2 determining the second-order bottom effects are given by

$$R_1 = \frac{1}{\cosh^2 kh} \left(W_1 I_1 + W_2 I_2 + W_3 I_3 + W_4 I_4 + W_5 I_5 + W_6 \right) \tag{2}$$

$$R_2 = \frac{1}{\cosh^2 kh} \left(U_1 I_1 + U_2 I_2 + U_3 I_3 \right). \tag{3}$$

The expressions of W_i, U_i, and I_i are given in the appendix of Suh et al. (1997), who found that there are minor algebraic errors in W_1 and W_2 of the Massel's equations. The wavenumber, k, is determined from the dispersion relation given by

$$\omega^2 = gk \tanh kh. \tag{4}$$

Eq. (1) is the same as the modified mild-slope equation developed by Chamberlain and Porter (1995). When the second-order bottom effect terms proportional to squared bottom slope, $(\nabla h)^2$, and bottom curvature, $\nabla^2 h$, are neglected in Eq. (1), it reduces to the mild-slope equation developed by Berkhoff (1972).

The linear wave theory gives the following relation between the velocity potential at mean water level, $\tilde{\phi}$, and the water surface elevation, η, as

$$\tilde{\phi} = -\frac{ig}{\omega} \eta = \frac{g}{\omega^2} \frac{\partial \eta}{\partial t} \tag{5}$$

where $i=\sqrt{-1}$ and g is the acceleration due to gravity. The volume flux $\mathbf{Q}$ defined by Copeland (1985) is given by

$$\mathbf{Q}=\frac{CC_g}{g}\nabla\tilde{\phi}. \tag{6}$$

Substitution of Eqs. (5) and (6) into the model Eq. (1) gives

$$\frac{\partial\eta}{\partial t}+\frac{1}{\frac{C_g}{C}-R_1(\nabla h)^2-R_2\nabla^2 h}\nabla\cdot\mathbf{Q}=0. \tag{7}$$

Taking the spatial and temporal derivatives of Eq. (5), with the use of Eq. (6), yields

$$\frac{\partial\mathbf{Q}}{\partial t}+CC_g\nabla\eta=0. \tag{8}$$

Eqs. (7) and (8) constitute a hyperbolic model which includes the terms of second-order bottom effects as an alternative to the elliptic model of Massel. Without the second-order bottom effect terms, Eqs. (7) and (8) reduce to the hyperbolic equations developed by Copeland (1985). Elimination of $\mathbf{Q}$ in Eqs. (7) and (8) yields

$$\frac{\partial^2\eta}{\partial t^2}-\frac{1}{\frac{C_g}{C}-R_1(\nabla h)^2-R_2\nabla^2 h}\nabla\cdot\left(CC_g\nabla\eta\right)=0. \tag{9}$$

which, if $R_1=R_2=0$, reduces to the hyperbolic equation of Copeland (1985) for a steady-state, harmonic solution.

3. Terms of second-order bottom effect

The terms of second-order bottom effects proportional to $(\nabla h)^2$ and $\nabla^2 h$ are included in the present model differently from the Copeland's model. The model Eq. (1) can be rewritten as

$$\nabla\cdot\left(CC_g\nabla\tilde{\phi}\right)+k^2CC_g\left\{1+E_1(\nabla h)^2+\frac{E_2}{k_o}\nabla^2 h\right\}\tilde{\phi}=0. \tag{10}$$

where $k_o=\omega^2/g$ is the deep-water wave number and the nondimensional values, E_1 and E_2, are

$$E_1=-\frac{C}{C_g}R_1 \tag{11}$$

$$E_2=-\frac{k_oC}{C_g}R_2. \tag{12}$$

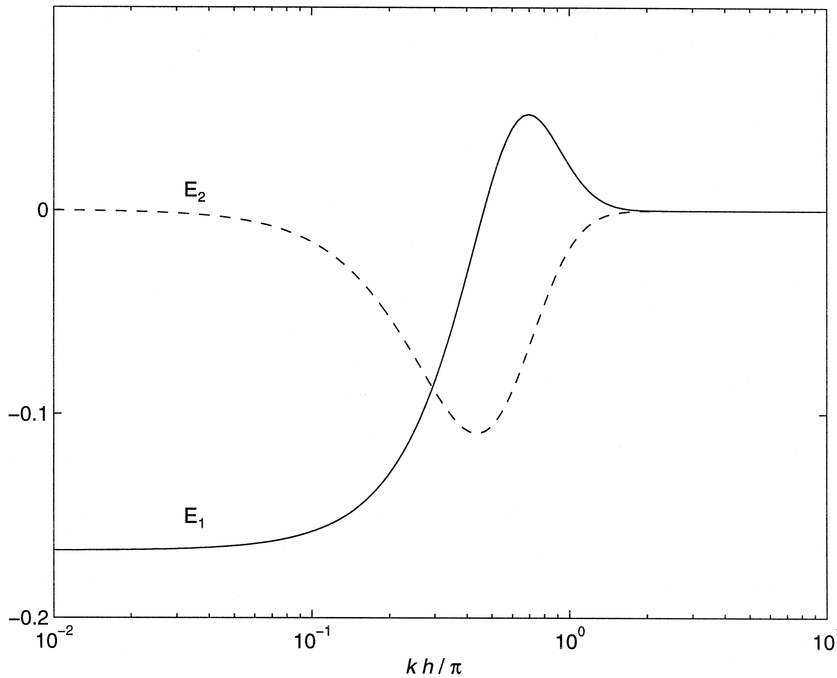

Fig. 1. Variations of E_1 and E_2 with kh; ———— $= E_1$, - - - $= E_2$.

As shown in Fig. 1, the effect of squared bottom slope expressed by E_1 is negligible in deep water $(kh > \pi)$, but it is non-negligible in intermediate-depth water and remains significant in shallow water $(kh < 0.1\pi)$. The effect of bottom curvature expressed by E_2 is negligible in both deep and shallow waters, but it is non-negligible in intermediate-depth water, being the most significant around $kh = 0.4\pi$. It is noticeable that E_1 is about zero when the effect of E_2 becomes maximum $(kh \simeq 0.4\pi)$, while E_2 approaches zero as E_1 exhibits the maximum effect $(kh < 0.1\pi)$.

4. Numerical tests

In order to examine the accuracy of the present model, we conduct numerical experiments with both the present model and the Copeland's model for monochromatic waves propagating over the plane slope with different inclination of Booij (1983). The reflection coefficients calculated by the models are compared against those by the finite element method (Suh et al., 1997). The two models are also tested for the case of waves propagating over the ripple patch of Davies and Heathershaw (1984). The calculated reflection coefficients are compared against the experimental data. Finally, the two models are tested for waves propagating over an arc-shaped bar with different angle at its front edge. The calculated reflection coefficients are compared against those by the eigenfunction expansion method.

4.1. Finite difference method

Waves are generated internally inside the model boundaries, while the waves propagating toward the wave generation point are permitted to freely pass across the point so that unwanted addition of wave energy in the model domain can be avoided. This technique, the so-called internal generation of waves, has been used by several coastal engineers (Larsen and Dancy (1983) for the Boussinesq equations; Madsen and Larsen (1987) and Yoon et al. (1996) for the model of Copeland (1985); Lee and Suh (1998) for the models of Radder and Dingemans (1985) and Copeland). In the present model and the Copeland's model, the value η^* added to the surface elevation at the wave generation point at each time step would be

$$\eta^* = 2\eta^I \frac{C\nabla t}{\Delta x} \tag{13}$$

where η^I is the water surface elevation of the incident wave, and Δx and Δt are the grid size and time step, respectively.

Sponge layers are placed at the outside boundaries to minimize wave reflection from the boundaries by dissipating wave energy inside the sponge layers. The thickness of the sponge layer, S, is taken as $2.5\times$ the local wavelength, which is found to reduce the magnitude of the incident wave to almost zero at the boundaries. In order to model the waves inside and outside the sponge layer continuously, Eq. (8) is modified as

$$\frac{\partial \mathbf{Q}}{\partial t} + CC_g \nabla\eta + \omega D_s \mathbf{Q} = 0. \tag{14}$$

The damping coefficient, D_s, is given by

$$D_s = \begin{cases} 0, & \text{outside sponge layer} \\ \dfrac{e^{d/S}-1}{e-1}, & \text{inside sponge layer} \end{cases} \tag{15}$$

where d is the distance from the starting point of the sponge layer.

If the value of $\{C_g/C - R_1(\nabla h)^2 - R_2\nabla^2 h\}$ becomes non-positive, Eq. (9) would be no longer of the type of wave equation and thus would not produce the phenomenon of wave propagation. Where the variation of the bottom topography is large, the magnitudes of $(\nabla h)^2$ and $\nabla^2 h$ can be large, and thus the value of $\{C_g/C - R_1(\nabla h)^2 - R_2\nabla^2 h\}$ can be non-positive. For example, at a sharp-cornered point, the magnitude of $\nabla^2 h$ is infinitely large, which, in intermediate-depth water, may make the solution of the present model invalid. In order to avoid such a troublesome case in the solution, we discretize the values of the squared bottom slope and the bottom curvature (in a one-dimensional domain) as

$$\left[\left(\frac{dh}{dx}\right)^2\right]_i = \left(\frac{h_{i+j}-h_{i-j}}{2j\Delta x}\right)^2 \tag{16}$$

$$\left[\frac{d^2h}{dx^2}\right]_i = \frac{h_{i+j}-2h_i+h_{i-j}}{(j\Delta x)^2} \tag{17}$$

where the subscript i denotes the spatial grid point where the above quantities are evaluated and j is selected as the minimum positive integer which guarantees a positive value of $\{C_g/C - R_1 (\nabla h)^2 - R_2 \nabla^2 h\}$.

In a one-dimensional domain, the modified models Eqs. (7) and (14) are discretized by a leap-frog method in a staggered grid in time and space, which yields

$$\frac{\eta_i^{n+1}-\eta_i^n}{\Delta t} + \frac{1}{\left[\frac{C_g}{C} - R_1\left(\frac{dh}{dx}\right)^2 - R_2\frac{d^2h}{dx^2}\right]_i}\frac{Q_{i+1}^n - Q_i^n}{\Delta x} = 0. \tag{18}$$

$$\frac{Q_i^{n+1}-Q_i^n}{\Delta t} + \left[CC_g\right]_{i-1/2}\frac{\eta_i^{n+1}-\eta_{i-1}^{n+1}}{\Delta x} + \omega\left[D_s\right]_{i-1/2}Q_i^n = 0. \tag{19}$$

where the superscript n denotes the time step. All the values of η and Q at the initial time step are set to be zero. For the slow start of wave generation, the left-hand side of Eq. (13) is multiplied by $\tanh(0.5t/T)$ where T is the wave period. At outside boundaries, perfect reflection is assumed, but the reflected wave becomes negligible inside the domain because the sponge layer significantly reduces the incoming wave energy. The time step is chosen for the minimum Courant number $C_r = C\Delta t/\Delta x$ to be 0.2 so that a stable solution is guaranteed.

4.2. Wave reflection from a plane slope

The models are tested for the case of waves propagating over a plane slope, each end of which is connected to a constant-depth region (see Fig. 2 for the computational domain for the numerical test). The constant water depths on the upwave and downwave sides of the slope are $h_1 = 0.6$ m and $h_2 = 0.2$ m, respectively, and the width of the slope, b, is varied so that the inclination of the slope varies. The wave period is 2 s. The grid spacing Δx is chosen for the minimum ratio of local wavelength to grid size to be 60 so that a spatial resolution is guaranteed. After a time of 30 T has elapsed since the initiation of wave generation, wave amplitudes in the region between $x = L_1$ and $x = 2L_1$ (L_1 = wavelength at depth h_1) are measured to calculate the reflection coefficient.

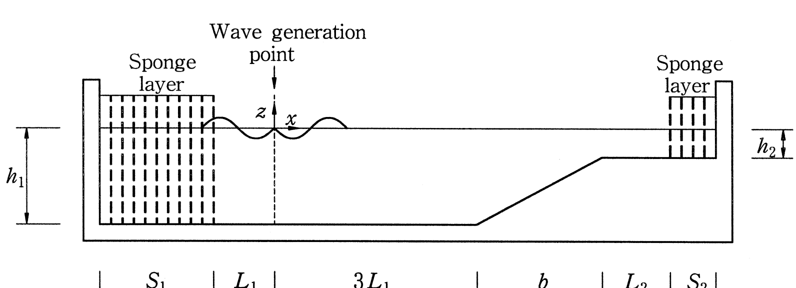

Fig. 2. Computational domain for numerical test of waves propagating over a plane slope.

Fig. 3 compares the present model, the Copeland's model, and the finite element model (Suh et al., 1997) results with respect to the slope width, b. It is shown that the present model gives reflection coefficients very close to those of the finite element model and the reflection coefficient becomes stable even for very steep slopes, while the Copeland's model underpredicts the reflection coefficient for steeper slopes. Even for very mild slopes, the present model and the Copeland's model show some difference, and the results of the finite element model coincide with those of the present model rather than the Copeland's model, though the reflection coefficients are very small there.

In order to examine the relative importance of the bottom slope square term and the bottom curvature term, additional calculations are made by including only the slope square term or the bottom curvature term to the Copeland's model. Each result is shown in Fig. 3 by a dashed line and dash–dotted line, respectively. As expected, the inclusion of the slope square term gives some difference from the Copeland's model for very steep slopes, but its effect is minor. On the other hand, the inclusion of the bottom curvature term improves significantly the Copeland's model so that the result follows closely that of the finite element model which is considered to be exact. Minor difference from the present model, which includes both the slope square term and the bottom curvature term, is observed only for very steep slopes where the effect of the

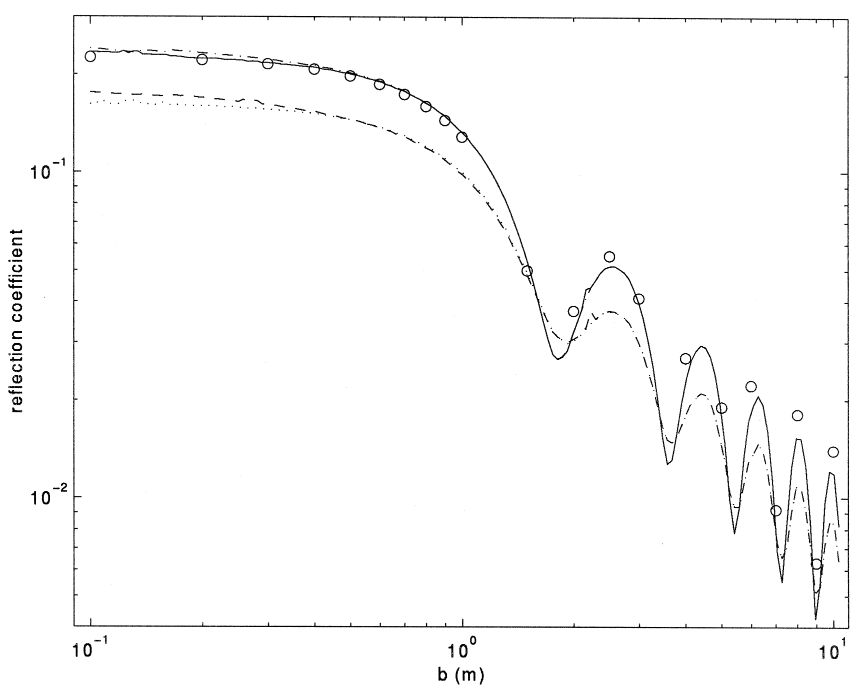

Fig. 3. Reflection coefficient vs. width of a plane slope; · · · = Copeland's model, - - - = Copeland's model plus bottom slope square term, - · - · - = Copeland's model plus bottom curvature term, ——— = present model, ○ = finite element solution.

slope square term becomes significant. As a result, the bottom curvature term is much more important than the bottom slope square term in this problem.

By comparison between the mild-slope equation and a finite element model for the aforementioned problem, Booij (1983) concluded that the mild-slope equation is sufficiently accurate up to the bottom slope of 1:3 without providing the finite element model results for the slopes milder than 1:3. This conclusion does not seem to be persuasive in terms of the bottom slope because of the following two reasons. First, it must be noticed that the slope tested is in water of intermediate depth ($0.15\pi < kh < 0.28\pi$) so that it does not cover the entire range of water depth from deep to shallow water. The accuracy of the mild-slope equation would vary with not only bottom slope but also water depth. Second, the slope tested includes two slope discontinuities, i.e., starting and end points of the slope, whose effect can be taken into account in the present equation by the bottom curvature term, which has been shown to significantly affect the solution. However, the mild-slope equation cannot take into account the effect of slope discontinuity.

4.3. Bragg reflection of waves from a sinusoidally varying topography

When waves propagate over a ripple patch, a significant portion of the wave energy is reflected from the ripple patch if the wavelength of the surface wave is around twice that of the ripple. This phenomenon is called the resonant Bragg reflection. The Bragg reflection becomes intensive with decreasing water depth, increasing ripple amplitude, and increasing number of ripples.

Davies and Heathershaw (1984) conducted a series of experiments with different numbers of ripples and water depths. In their experiment, the ripple wavelength and amplitude were 1 m and 5 cm, respectively, and the number of ripples was 2, 4, and 10. The water depth at the constant-depth region was 15.6 cm for the cases of 2 and 4 ripples and 31.3 cm for the case of 10 ripples. This experimental data has been used for comparison with various numerical models by a number of researchers including Kirby (1986), Massel (1993), Chamberlain and Porter (1995), and Suh et al. (1997). All of them showed that the mild-slope equation gives a good agreement with the experimental data for the cases of 2 and 4 ripples, but, for the case of 10 ripples, it fails to predict the magnitude of Bragg reflection. Therefore, in the present study, a numerical test is made only for the case of 10 ripples.

The computational domain for the numerical test is shown in Fig. 4. The water depth is given by

$$h(x) = \begin{cases} h_c, & x - x_s \le 0 \\ h_c - A\sin[K(x - x_s)], & 0 \le x - x_s \le n\lambda \\ h_c, & x - x_s \ge n\lambda \end{cases} \tag{20}$$

where A is the ripple amplitude, λ is the ripple wavelength, n is the number of ripples, h_c is the water depth at the constant-depth region, K is the wavenumber of the ripple, and x_s is the x-coordinate of the starting point of the ripple patch. The grid size Δx is chosen to be $\lambda/30$. The ratio, $2k/K$, is varied from 0.5 to 2.5 which, with the given

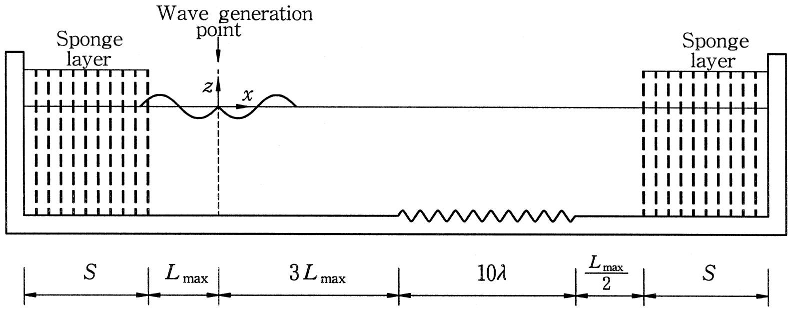

Fig. 4. Computational domain for numerical test of waves propagating over a ripple patch.

ripple wavelength, determines the wavelength of surface waves. For the shortest wave to be tested (i.e., $2k/K = 2.5$), one wavelength contains $24\Delta x$. After a time of 70 T has elapsed since the initiation of wave generation, wave amplitudes in the region between $x = L_{max}$ and $x = 2L_{max}$ (L_{max} = wavelength on the flat bottom with $2k/K = 0.5$) are measured to calculate the reflection coefficient.

Fig. 5 shows the reflection coefficients calculated by the present model and the Copeland's model along with the experimental data. Again, in order to examine the

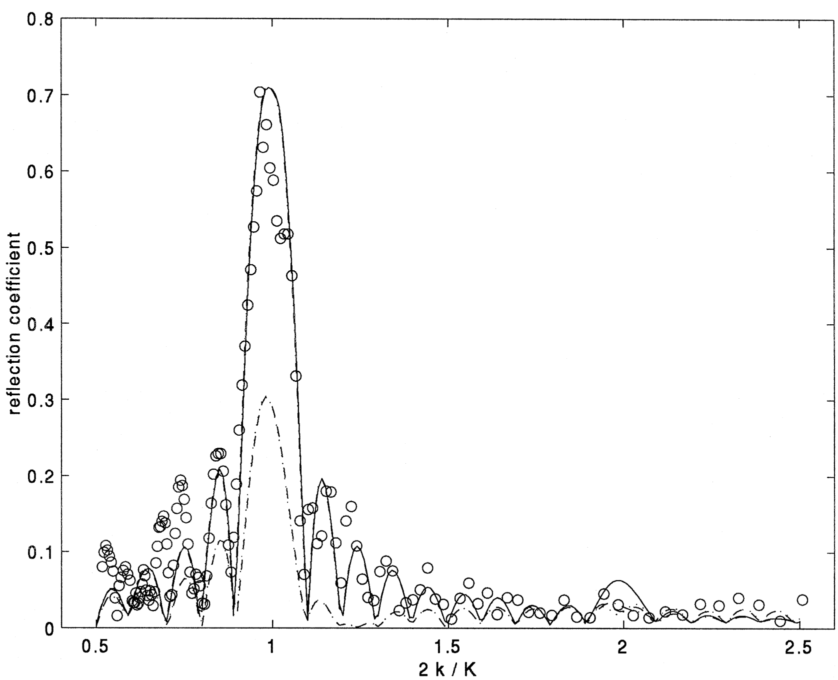

Fig. 5. Reflection coefficient as function of $2k/K$ from ripple bed; · · · = Copeland's model, - - - = Copeland's model plus bottom slope square term, - · - · - = Copeland's model plus bottom curvature term, ———— = present model, ○ = experimental data.

relative importance of the bottom slope square term and the bottom curvature term, the results of the Copeland's model including only the slope square term or the bottom curvature term are also presented in Fig. 5. The results of the present model and the Copeland's model including only the bottom curvature term show some difference only in the vicinity of $2k/K = 2.0$, and for other values of $2k/K$ they are almost identical so that the difference is undistinguishable in the figure. Both the present model and the Copeland's model including only the bottom curvature term describe the resonant peak very well. The Copeland's model and that including only the slope square term (shown to be almost identical in the figure), however, while correctly positioning the resonant reflection, completely fail to predict its magnitude. Some of the researchers have interpreted this failure to be attributed to the violation on the mild-slope assumption that the depth must vary slowly over a wavelength. However the results shown in Fig. 5 suggest that this interpretation is not appropriate. The failure of the Copeland's model (equivalently the mild-slope equation) may be not because the depth varies rapidly but because it does not include the effect of bottom curvature. It is also worthwhile to note that, for this Bragg problem, the depth perturbation about the mean bed level is of the form of $A\sin(Kx)$ so that $(dh/dx)^2 = O(\varepsilon^2)$ and $d^2h/dx^2 = O(\varepsilon)$ where $\varepsilon = A/\lambda \ll 1$. Therefore, as for the Bragg problem, the bottom curvature term may be much more important than the slope square term.

4.4. Wave reflection from an arc-shaped bar

Finally, the two models are tested for waves propagating over an arc-shaped bar with different angle at its front edge. Fig. 6 shows the computational domain for the test. The water depth is given by

$$h(x) = \begin{cases} h_c + \dfrac{r}{\tan\theta} - \sqrt{\left(\dfrac{r}{\sin\theta}\right)^2 - (x-x_0)^2}, & |x-x_0| \le r \\ h_c, & |x-x_0| \ge r \end{cases} \tag{21}$$

where the water depth on the flat bottom, h_c, is 85 cm, the half-width of the arc, r, is 80 cm, and x_0 is the x-coordinate at the center of the arc. The water depth on the bar can be deduced from the geometric relations given by $h = h_c - z_2$ and $z_1 + z_2 = \sqrt{R^2 - (x-x_0)^2}$, where $z_1 = r/\tan\,\theta$ and $R = r/\sin\,\theta$. The angle at the front edge of the bar, θ, is varied from 0° to 90° and thus the water depth at the center of the bar is varied from 85 cm to 5 cm. The wave period is chosen to be 1.716 s so that the relative water depth at the flat bottom is $kh_c = 0.42\pi$ and thus the effect of bottom curvature caused by the sharp-cornered front edge of the bar becomes prominent (see Fig. 1). The higher-order bottom effects can be analytically obtained as $(\nabla h)^2 = (x-x_0)^2/\{(r/\sin\,\theta)^2 - (x-x_0)^2\}$ and $\nabla^2 h = \{2(r/\sin\,\theta)^2 - (x-x_0)^2\}/\{(r/\sin\,\theta)^2 - (x-x_0)^2\}^{3/2}$ both of which, at the edge of the bar, would increase infinitely as the front angle, θ, increases up to 90°. In this study, however, the terms of these two effects are obtained by discretization as in Eqs. (16) and (17) in order to get a positive value of $\{C_g/C - R_1(\nabla h)^2 - R^2\nabla^2 h\}$. The grid size, Δx, is taken to be 2.5 cm so that the

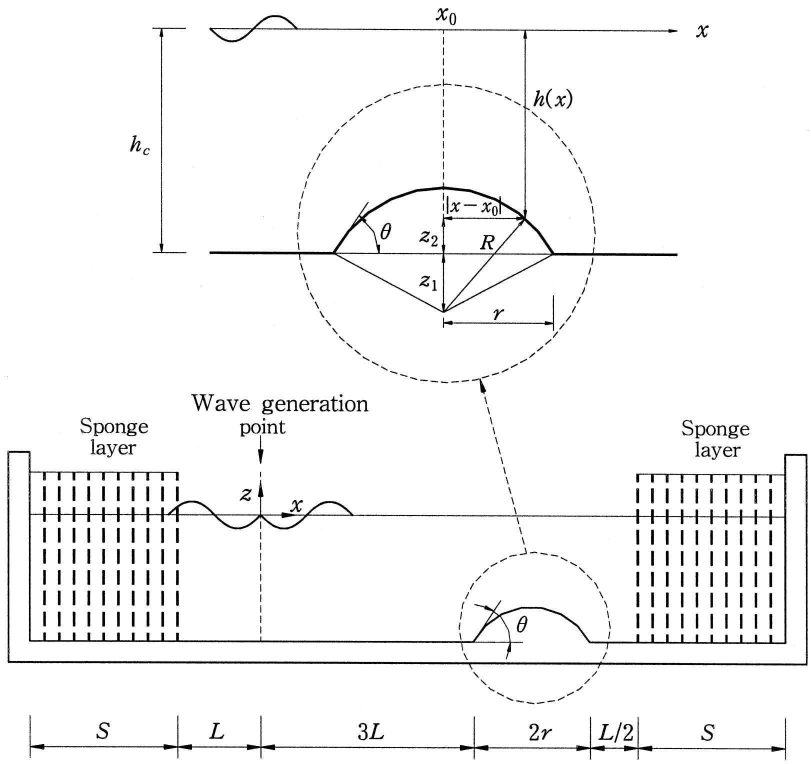

Fig. 6. Computational domain for numerical test of waves propagating over an arc-shaped bar.

minimum ratio of the local wavelength to the grid size becomes 47. After a time of 20 T has elapsed since the initiation of wave generation, wave amplitudes in the region between $x = L_c$ and $x = 2L_c$(L_c = the wavelength on the flat bottom) are measured to calculate the reflection coefficient.

As mentioned in the introduction, when the bottom topography is simple, the transformation of water waves can be predicted with high accuracy by using a finite element method or an eigenfunction expansion method. For this problem of wave reflection from an arc-shaped bar, the results of the present model and the Copeland's model are compared against that of the eigenfunction expansion method. Although the eigenfunction expansion method can easily include not only the propagating wave mode but also the evanescent modes generated at each discontinuity between neighboring shelves, the evanescent modes are not included in this calculation for the purpose of direct comparison with the present model and the Copeland's model which do not include the evanescent modes.

Fig. 7 shows the comparison of the reflection coefficients calculated by the aforementioned models. Both the present model and the eigenfunction expansion method shows that, as the angle at the front edge increases, the reflection coefficient increases up to

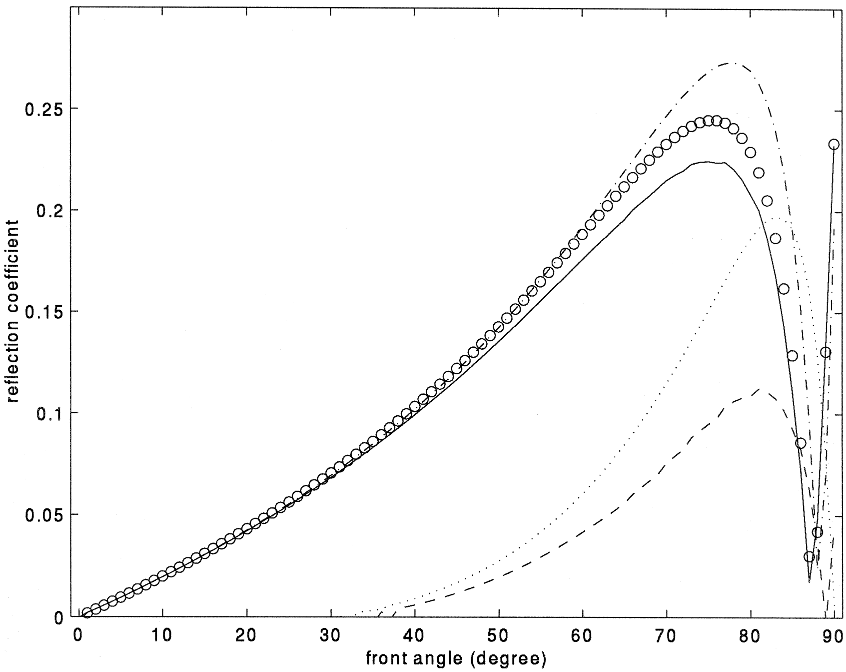

Fig. 7. Reflection coefficient vs. front angle of an arc-shaped bar; ··· = Copeland's model, --- = Copeland's model plus bottom slope square term, -·-·- = Copeland's model plus bottom curvature term, ——— = present model, ○ = eigenfunction expansion method.

$\theta = 75°$, and then decreases to almost zero till $\theta = 87°$, and after that it increases again till $\theta = 90°$. This interesting phenomenon seems to resulted from the combined effects of the magnitude and phase of the reflected wave at each point of depth change. The significant reflection at $\theta = 75°$ and zero reflection at $\theta = 87°$ in this case would be compared to the Bragg reflection and zero reflection, respectively, of waves by a ripple patch. For the Copeland's model, the reflection coefficient increases up to $\theta = 82°$ and then decreases to zero till $\theta = 90°$. On the whole, the reflection coefficient calculated by the present model closely follows that by the eigenfunction expansion method except a slight difference around $\theta = 75°$, while the reflection coefficient calculated by the Copeland's model is quite different from those by the other two models. This difference may be resulted from the fact that the Copeland's model does not include the second-order bottom effect terms.

Again the Copeland's model is tested by including only the bottom slope square term or the bottom curvature term. The results are shown in Fig. 7. When the bottom curvature term is included, the model result becomes much closer to those of the eigenfunction expansion method than the present model, especially for smaller front angles of the bar. The inclusion of the slope square term, however, rather deteriorates the solution though it simulates the bounce of the reflection coefficient at a large θ somewhat incorrectly.

5. Conclusions

A hyperbolic wave equation model has been developed for waves propagating over a rapidly varying topography based on the extended refraction–diffraction equation of Massel (1993), which is expressed in an elliptic form. The model developed is an extension of the model of Copeland (1985) for the application to a rapidly varying topography by the inclusion of the bottom slope square term and the bottom curvature term. By examining these additional terms with respect to various relative water depths, it has been shown that the bottom slope square term is negligible in deep water but it is not in both intermediate-depth water and shallow water. On the other hand, the bottom curvature term is negligible in both deep and shallow waters, while its effect is significant in intermediate-depth water.

In order to examine the importance of these additional terms, the present model and the model of Copeland (1985) were tested for the problems of wave reflection from a plane slope, periodic ripples, and an arc-shaped bar. In addition, in order to compare the relative importance of these terms, the Copeland's model plus the bottom slope square term or the bottom curvature term was tested for the same problems. The results of the various models were compared with those of the finite element method or the eigenfunction expansion method which are considered to give a highly accurate solution. For all the problems tested, the present model (including both the bottom slope square term and the bottom curvature term) has been shown to give reasonably accurate results, while the Copeland's model fails to predict major characteristics of the problems. It has also been shown that the bottom curvature term plays an important role in improving the model results, while the effect of the bottom slope square term is minute.

In most practical problems, the Copeland's model plus only the bottom curvature term may give sufficiently accurate results. However, there is no reason for not using the model developed in this study, which includes the bottom slope square term as well, because its use may require only a little increase of computing time or effort.

One of the advantages of a hyperbolic model compared to an elliptic model may be the reduction in computing time, especially in a two-dimensional domain. However, appropriate experimental data in a two-dimensional domain for proving the superiority of the present model are rare. Recently, Chandrasekera and Cheung (1997) have applied a model in the same class as the present one to wave transformation over a circular shoal with a relatively steep side slope for which experimental data were reported by Williams et al. (1980). However, these experimental data do not seem to be appropriate to corroborate the effects of the additional terms in the present model. In this context, a two-dimensional hydraulic model test may be necessary in the future.

References

Berkhoff, J.C.W., 1972. Computation of combined refraction–diffraction. In: Proc. 13th Coastal Eng. Conf., Vancouver, Vol. 1, pp. 471–490.

Booij, N., 1981. Gravity waves on water with non-uniform depth and current. Rep. No. 81-1, Dept. of Civ. Eng., Delft Univ. of Technology.

Booij, N., 1983. A note on the accuracy of the mild-slope equation. Coastal Eng. 7, 191–203.

Chamberlain, P.G., Porter, D., 1995. The modified mild-slope equation. J. Fluid Mech. 291, 393–407.

Chandrasekera, C.N., Cheung, K.F., 1997. Extended linear refraction–diffraction model. J. Waterw. Port Coastal Ocean Eng. 123, 280–286.

Copeland, G.J.M., 1985. A practical alternative to the mild-slope wave equation. Coastal Eng. 9, 125–149.

Davies, A.G., Heathershaw, A.D., 1984. Surface-wave propagation over sinusoidally varying topography. J. Fluid Mech. 144, 419–443.

Kirby, J.T., 1986. A general wave equation for waves over rippled beds. J. Fluid Mech. 162, 171–186.

Larsen, J., Dancy, H., 1983. Open boundaries in short wave simulations—a new approach. Coastal Eng. 7, 285–297.

Lee, C., Suh, K.D., 1998. Internal generation of waves for time-dependent mild-slope equations. Coastal Eng. (in press).

Madsen, P.A., Larsen, J., 1987. An efficient finite-difference approach to the mild-slope equation. Coastal Eng. 11, 329–351.

Massel, S.R., 1993. Extended refraction–diffraction equation for surface waves. Coastal Eng. 19, 97–126.

Miles, J.W., 1967. Surface-wave scattering matrix for a shelf. J. Fluid Mech. 28, 755–767.

Nishimura, H., Maruyama, K., Hiraguchi, H., 1983. Wave field analysis by finite difference method. In: Proc. 30th Japanese Conf. Coastal Eng., Tokyo, pp. 123–127 (in Japanese).

Radder, A.C., Dingemans, M.W., 1985. Canonical equations for almost periodic, weakly nonlinear gravity waves. Wave Motion 7, 473–485.

Smith, J., 1983. On surface gravity waves crossing weak current jets. J. Fluid Mech. 134, 277–299.

Smith, R., Sprinks, T., 1975. Scattering of surface waves by a conical island. J. Fluid Mech. 72, 373–384.

Suh, K.D., Lee, C., Park, W.S., 1997. Time-dependent equations for wave propagation on rapidly varying topography. Coastal Eng. 32, 91–117.

Takano, K., 1960. Effets d'un obstacle parallélépipédique sur la propagation de la houle. Houille Blanche 15, 247–267.

Williams, R.G., Darbyshire, J., Holmes, P., 1980. Wave refraction and diffraction in a caustic region: a numerical solution and experimental validation. Proc. Inst. Civ. Eng. 69, 635–649.

Yeung, R.W., 1975. A hybrid integral-equation method for time-harmonic free-surface flow. In: Proc. 1st Int. Conf. Num. Ship Hydrodynamics, pp. 581–607.

Yoon, S.B., Lee, J.I., Lee, J.K., Chae, J.W., 1996. Boundary treatment techniques of numerical model for the prediction of harbor oscillation. J. Korean Soc. Civ. Eng. 16, 53–62 (In Korean).